Coda of Long-Range Arrivals from Nuclear Explosions

Article *in* Bulletin of the Seismological Society of America · September 2000

DOI: 10.1785/0119990125

2 authors, including:

Scott B. Smithson
University of Wyoming
177 PUBLICATIONS **4,024** CITATIONS

SEE PROFILE

Bulletin of the Seismological Society of America, 90, 4, pp. 929–939, August 2000

Coda of Long-Range Arrivals from Nuclear Explosions

by Igor B. Morozov and Scott B. Smithson

Abstract Short-period, three-component recordings from peaceful nuclear explosions (PNE) of the profile QUARTZ, located in Russia, are used to constrain the nature of the coda of PNE arrivals. In particular, we examine the unusually strong and extensive coda of the long-range P_n (interpreted as a whispering-gallery, WG) phase propagating to beyond 3000 km. Energy-balance considerations in three dimensions show that such an extensive coda is inherent not only to WG but to all other *P*-wave phases and can be explained by crustal scattering. The long coda is a result of excitation of short-period scattered waves (*Pg, Sg, Lg, Rg*) within the crust by the waves incident from the mantle, or, conversely, by generation of mantle phases from crustal guided waves within the source region. The resulting estimates of coda Q range between $Q = 380$ near 2 Hz and $Q = 430$ near 5 Hz and can be associated with crustal attenuation including the sediments. Our coda model also explains quantitatively the observed build-up of the arrival amplitude with time and the apparent lack of a pronounced coda of the body-wave arrivals from the mantle transition zone. These effects result from adding up the energy of the later arrivals arriving during the codas of earlier arrivals. We "deconvolve" the overlapping coda patterns and show that the true relative energies of the arrivals are significantly lower than the apparent energies measured from the raw records. A whispering-gallery interpretation of the long-range P_n and crustal scattering accounts for the entire range of observations of kinematic, spectral, and amplitude pattern of the PNE wavefield and allows the derivation of constraints on attenuation.

Introduction

Seismic studies, including deep refraction and reflection experiments using large chemical and nuclear explosions, have demonstrated strong heterogeneity of the uppermost mantle. Mantle heterogeneity is manifested in velocity contrasts and pronounced stratification of the lithosphere imaged by *P*/*S* wave conversions (e.g., Bostock, 1998), in mantle reflectivity (e.g., Pavlenkova, 1996; Morozova *et al.,* 1999), and in variations of seismic attenuation (e.g., Der *et al.,* 1986; Morozov *et al.,* 1998a, 1998b). Mantle velocity gradients and reflecting boundaries form a relatively shallow (between 100 and 150 km depth) waveguide favoring propagation of seismic energy to teleseismic distances of up to 3000 km (Figs. 1 and 2, Mechie *et al.,* 1993; Ryberg *et al.,* 1995; Morozov *et al.,* 1998a). Such phases, known as long-range (teleseismic) P_n, were also identified in long-range profiles using large conventional explosions (Enderle *et al.,* 1997; Henstock *et al.,* 1998) and acquired critical significance for some interpretations of the fine-scale structure of the uppermost mantle (e.g., Enderle *et al.,* 1997). Since these waves are confined within the uppermost 100–120 km of the mantle, amplitude and coda character carry important information about the structure of this region.

Two recent interpretations of the long-range P_n sharply diverge in their interpretations of the observations and in conclusions about the uppermost mantle structure. Based on one-dimensional (1D) modeling of coda properties using the method by Fuchs and Müller (1971), Tittgemeyer *et al.* (1996), and Ryberg and Wenzel (1999) proposed a special, "high-frequency waveguide" propagation mechanism of the long-range P_n. These authors suggested a small-scale, random sub-Moho layering with high, 5% velocity fluctuations and average layer thickness of 2 km within a zone extending 75 km below the Moho (Ryberg and Wenzel, 1999). Although faced with significant difficulties in petrologic interpretation of this model (e.g., Ryberg and Wenzel, 1999, p. 10,660), such strongly scattering uppermost mantle was viewed as a global phenomenon (Enderle *et al.,* 1997).

In contrast to the aforementioned model, Morozov *et al.* (1998a) argued that the observations of the long-range P_n could be better explained by multiple sub-Moho refractions (whispering-gallery modes) within the uppermost mantle. According to this interpretation, no unusual wave-propagation mechanism was required in order to explain the nature of this phase and no strong scattering within the uppermost mantle is required. At larger ranges, similar strong *PP* phases

followed by extensive codas were identified in NORSAR recordings of nuclear explosions in Western Russia (Baumgardt, 1985). The enhanced high-frequency content of these phases relatively to the waves diving into the mantle transition zone was explained by increased attenuation below a depth of about 150 km (Morozov *et al.,* 1998a,b). Morozov *et al.* (1998a) and Morozov (in press) argued that the "scattering waveguide" model was primarily based on a misinterpretation of the apparently high-frequency character of the long-range P_n by Ryberg *et al.* (1995) and by the inadequate, 1D models of its coda employed by Tittgemeyer *et al.* (1996) and Ryberg and Wenzel (1999).

Although kinematic behavior and spectral content of the long-range P_n does not present any difficulty for the whispering-gallery model (Morozov *et al.,* 1998a), the high amplitude of this phase and particularly its extensive coda (Fig. 2) still need to be understood. Recent studies of the decay rate of this coda resulted in surprisingly high values of coda Q between 1000 and 2000 (Ryberg and Wenzel, 1999) or even 2000 and 5000 (Ryberg *et al.,* 1995). Such high Q values can hardly be associated with crustal attenuation, and as a result, extremely strong yet horizontally coherent scattering within the mantle was suggested (Ryberg *et al.,* 1995).

Although numerical modeling of three-dimensional (3-D) scattering effects of short-period PNE wavefields still presents insurmountable difficulties, scattering is still inherently a multidimensional process, and only accounting for 3D wave propagation can explain the observed coda decay rate. Fortunately, the observed coda amplitude pattern allows an explanation from simple physical considerations of energy balance; such an explanation is the focus of the present study.

For our interpretation of the long-range P_n amplitude, we extract amplitude decay curves within 200 sec of a range of seismic records from PNE QUARTZ-4 (often referred to as PNE 323) where the separation of the phases provides the best illustration of the QUARTZ PNE energy pattern (Figures 1 and 3, modified from Morozov *et al.,* 1998a). The energy in the PNE wavefield at this distance appears to build up for 20–30 s after the first arrivals, followed by an extensive coda that can be observed for 100–150 sec (Fig. 3). Both the high amplitudes of the WG phases and the coda are surprising and do not fit into conventional views. Specifically, we will seek answers to two intriguing problems of the recorded distribution of PNE energy (Fig. 3):

1. What is the nature and decay character of the observed codas of PNE arrivals? Why is the coda of the free-surface multiple *PP* (WG_{fs} in our notation) much stronger than the coda of $P_{410}P$ reflections of nearly the same amplitude?
2. Why are the amplitudes of the WG phases so high compared to the reflections from the transition zone, whereas 1D modeling shows much lower amplitudes (synthetic models were presented by Mechie *et al.,* 1993, and Morozova *et al.,* 1999).

These are precisely the questions put forward in support of the "scattering waveguide" interpretation by Ryberg and others; however, we emphasize that there is very little of a specific, "high-frequency" accent in these questions. Instead, these problems are more clearly posed by the low-frequency, high-amplitude pattern in Figure 3. Note that the "scattering waveguide" model by Ryberg *et al.* (1995) is based solely on the high-frequency coda of *WG,* whereas the low-frequency coda is stronger and longer, indicating that the scattering phenomenon is broadband and cannot be attributed to a tuned, high-frequency scattering within the uppermost mantle. Also, unlike the aforementioned authors, we consider the crust, as the most structurally and compositionally complex part of the Earth, also the most likely source of seismic scattering.

As we show in the following sections, a simple physical model of the coda allows us to obtain meaningful estimates of crustal attenuation quality factor (Q) and of the relative amplitudes of the arrivals without presently impractical 3D finite-difference modeling. Our approach follows coda models accepted in teleseismic array observations (e.g., Greenfield, 1971; Bannister *et al.,* 1990; Dainty, 1990; Gupta *et al.,* 1991) and is based on two fundamental observations. Firstly, waves propagating through the mantle and incident on the crust at high apparent velocity form a source of scattered energy different from the point-source model commonly used in coda estimates. Thus a correct coda model must take into account the distributed character of its excitation. Secondly, despite their apparent difference, we postulate that all the mantle arrivals could have similar coda patterns. Due to their long extent, these codas overlap, creating the stepwise increase in energy seen in Figure 3. Decomposition of the recorded amplitude pattern allows us to obtain the true relation between the amplitudes of the onsets of the different PNE phases and their codas.

Coda decay rate of the long-range PNE arrivals

Figure 3 shows that the two *WG* multiples forming the long-range P_n are clearly distinct in the character of their codas. The first, Moho multiple labeled *WG* in Figure 3 is followed by a coda that dominates the high-frequency record (Fig. 2). However, in the low-frequency band, the strongest phase is the free-surface P_n multiple (WG_{fs}) followed by its coda. The higher amplitude of the WG_{fs} event is consistent with higher reflectivity of the free surface compared to the Moho. Also, the longer and low-frequency coda of WG_{fs} suggests a predominance of surface waves that propagate efficiently at lower frequencies and are progressively more attenuated as the frequency increases.

Previous measurements of coda decay rate by Ryberg *et al.* (1995) and Ryberg and Wenzel (1999) resulted in two conflicting estimates, both of which suggested very high Q values over 1000–2000. However, values of Q might be overestimated from the use of a coda power decay rate (Aki and Chouet, 1975):

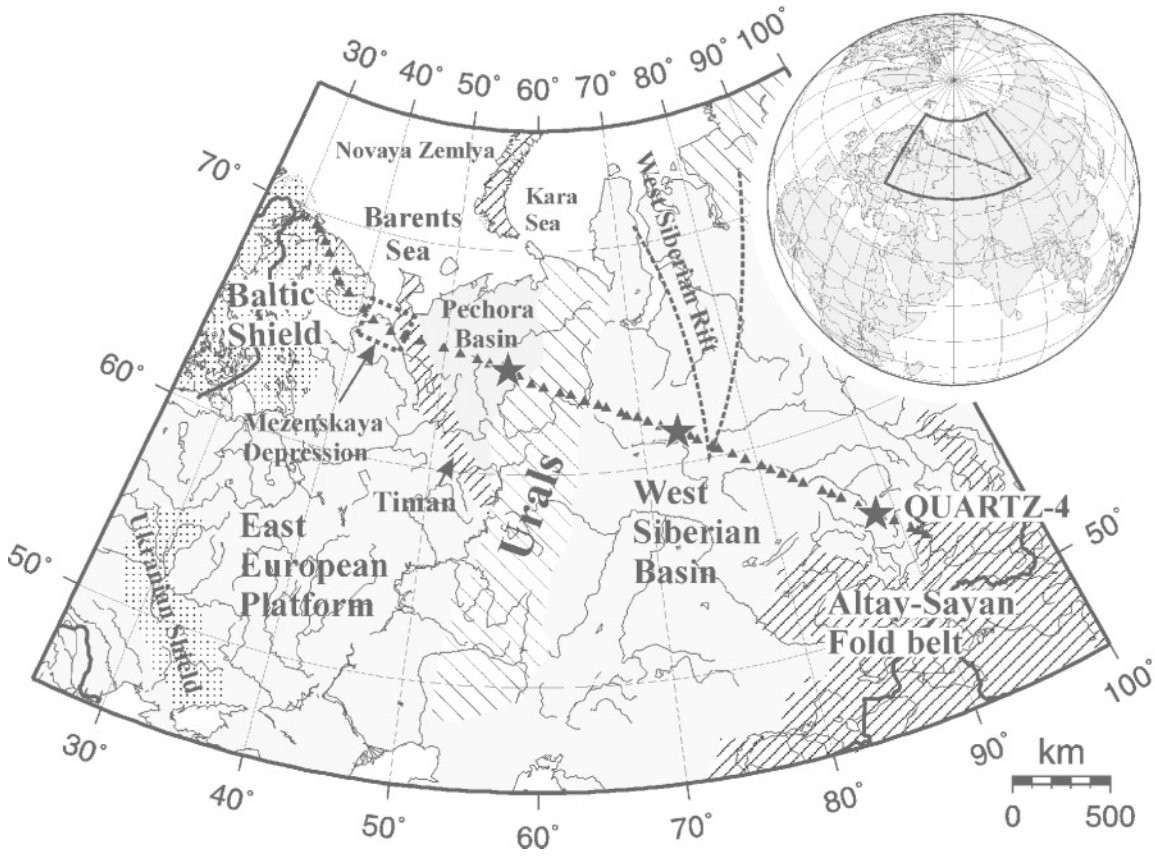

Figure 1. Map of the western part of the former USSR showing the profile QUARTZ. Triangles and stars indicate the locations of the chemical and nuclear explosions (PNEs) recorded by the profile, respectively, and PNE QUARTZ-4 is labeled. This PNE presents one of the best examples of the long-range P_n (Fig. 2). Major tectonic structures crossed by the profile are indicated. Dotted box near the Mezanskaya depression indicates the location of the receivers used in coda decay measurements in this study.

$$P(t) \propto t^{-\zeta} e^{-\omega t/Q}, \quad (1)$$

where t is the time after the arrival, ω is the frequency. In expression (1), the factor $t^{-\zeta}$ with $\zeta \geq 1$ describes the geometric spreading of the waves forming the coda, and the quality factor Q corresponds to the attenuation. Ryberg and Wenzel (1999) used a preset value of $\zeta = 2$ assuming body-wave nature of the coda waves and a point source. However, as pointed out by Morozov *et al.* (1998a) and Morozov (in press), the energy of the coda of the long-range PNE phases is better described by a relation (1) with $\zeta \approx 1.0$ for the higher-frequency coda and $\zeta \approx 0.9$ for the lower-frequency coda, with $Q = \infty$. This ambiguity in the determination of the attenuation factor Q using equation (1) illustrates the importance of a correct model of geometrical spreading. The tendency of the geometric spreading parameter ζ to values lower than 1 when $Q = \infty$ shows that formula (1) may not be applicable to the coda decay rate of the long-range PNE arrivals.

Assuming predominantly crustal origin of the coda waves, coda amplitudes of PNE arrivals in Figure 3 can be explained readily once we take into account that seismic waves propagating through the mantle and entering the crust form a source of scattered waves that is different from a point source implied by relation (1). High apparent velocity of the incident waves (8–10 km/sec) exceeds the velocity of the crustal-guided waves (3.5–5.5 km/sec) generated through conversions on the Moho, on the basement, on surface topography, and on other velocity heterogeneities. Note that the most efficiently propagating phases within the crust (in the frequency range 0.5–10 Hz), postcritically reflected *S* waves, or *Lg* (Campillo, 1987), tend to the lower limit of this velocity range. High velocity of the moving source of scattered waves leads to a distributed source of coda energy.

In order to derive a phenomenological model of PNE coda excitation, we assume for simplicity that the coda of a PNE arrival consists predominantly of *Lg*; however, the argument should hold for other types of waves trapped within the crust. A commonly used *Lg* amplitude decay relation (e.g., Campillo, 1987; McNamara *et al.,* 1996) converted to power units is:

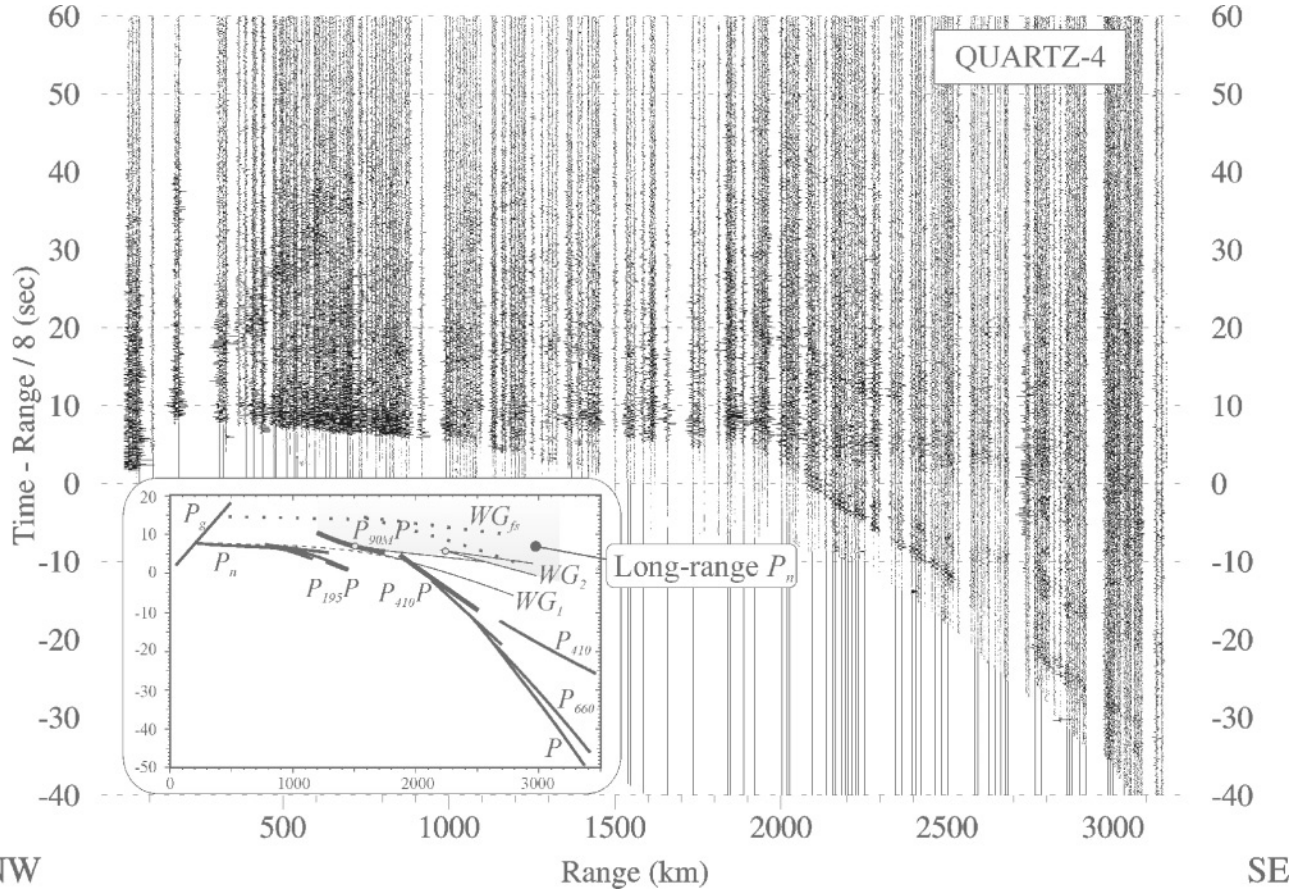

Figure 2. Vertical-component record from PNE QUARTZ-4 (Figure 1; this explosion is also often referred as PNE 323). Inset shows a sketch of refracted, reflected arrivals and their multiples identified in this complex wave pattern. The long-range P_n phase (shaded in the inset) consists of a variety of arrivals forming a strong band of energy propagating to 3000 km at a group velocity between 8.0 and 8.1 km/sec, with a faster branch at 8.5 km/sec beyond 2700 km (Morozov *et al.,* 1998a). Frequency content of this phase is close to that of the ordinary P_n (Morozov *et al.,* 1998a), and after a high-pass filtering removing the deeper mantle body waves, this phase dominates the record (Ryberg *et al.,* 1995). Note the unusually high energy of the arrivals in the primary P_n branch supporting the interpretation of the long-range P_n as a series of Moho and free-surface multiples of P_n and P_N (WG and WG_{fs}). Also note that the long-range P_n phase is strong and is followed by a coda extending beyond the ends of records shown here (Figure 3).

$$P(f,\ D)\ =\ \frac{1}{D^{2\gamma}}\ R(f)S(f)e^{-2\pi fD/vQ(f)}, \qquad (2)$$

where D is the hypocentral distance, R and S are receiver and source terms describing site effects at the recording and excitation points, respectively, f is the median frequency of the observed wave, v is the group velocity for Lg, γ is the exponent of the geometric spreading within the medium, and Q is the quality factor of Lg propagation within the crust. Since the duration of Lg increases with distance, γ is larger than the value of 0.5 used for regional surface waves (Frankel *et al.,* 1990), and a value of $\gamma = 0.83$ is generally accepted for Lg amplitude measurements in the time domain (Campillo, 1987, 1990; McNamara, 1996).

The expression (2) gives Lg power at distance D from the excitation point. By multiplying this expression by a time windowing function ("wavelet power") $W(t-t_0,\ D)$ we transform it into a phenomenological time distribution of recorded Lg power at time t:

$$P(t,\ D)\ =\ \frac{W(t\ -\ t_0,\ D)}{D^{2\gamma}}\ RSe^{-2\pi fD/vQ}, \qquad (3)$$

where t is the recording time, t_0 is the Lg generation time (onset of the mantle arrival at the scatterer), and we have ignored the frequency dependence for simplicity. The function $W(t-t_0,\ D)$ describes the broadening of the Lg wavetrain of an original duration τ at larger distances, and can be approximated as:

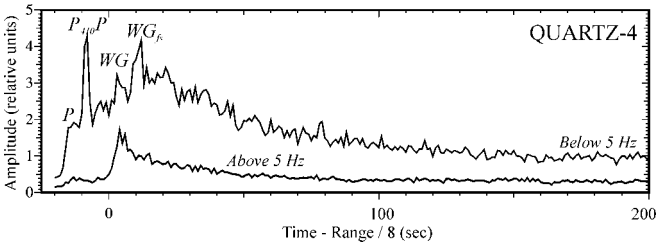

Figure 3. Amplitude of the high-frequency and low-frequency (filter corner frequency is 5 Hz in both cases) records within the offset range 2500–2600 km from PNE QUARTZ-4 (modified from Morozov *et al.,* 1998a). Time reduction is 8 km/sec, and 7 three-component instantaneous trace amplitude records were averaged within a 2-sec sliding time window and within the offset range (Morozov and Smithson, 1996) was used. First arrivals, a reflection from the 410-km discontinuity, and two whispering-gallery phases (*WG* and WG_{fs}) are indicated. Note the difference of the codas following the free-surface multiple refraction WG_{fs} at low frequencies and the Moho multiple *WG* at high frequencies.

$$W(t - t_0, D) = \begin{cases} 1 \text{ for } \dfrac{D}{v} < t - t_0 < \dfrac{D}{v} + \tau D^{2\gamma-1}, \\ 0 \text{ otherwise.} \end{cases} \quad (4)$$

Relation (4) ensures energy balance in equation (3) without attenuation.

By integrating the recorded *Lg* power at recording point $\mathbf{r}$ and at time t over all source (scattering point) locations, we obtain an expression for the recorded coda power:

$$P(\mathbf{r}, t) = R \int d^2\mathbf{r}_s \frac{W\left(t - \dfrac{|\mathbf{r}_s|}{v_a}, D\right)}{D^{2\gamma}} S(\mathbf{r}_s)\, e^{-2\pi f D/vQ}, \quad (5)$$

where $\mathbf{r}_S$ is the surface integration point, v_a is the apparent velocity of the arrival generating the coda, $D = |\mathbf{r} - \mathbf{r}_S|$, and $S(\mathbf{r}_S)$ is the scattering power proportional to the incident wave power (Fig. 4). Note that at a given time t, the recorded coda is built up of the waves scattered from within a ring *around* the recording point (Fig. 4); the area of this ring increases with time due to its increasing radius and width.

In a simple approximation corresponding to our averaged measurement of coda decay (Fig. 3), we assume in relation (5) $|\mathbf{r}_S|/v_a \ll D/v$ and $S(\mathbf{r}_S) \approx$const, corresponding to a nearly simultaneous generation of scattered energy within the crust and on the Moho. The integration area in Figure 4 then becomes circular, and the geometric spreading and the time window factors cancel. Therefore, instead of relation (1), the coda of a PNE arrival is better described by a simple exponential expression (with $\omega = 2\pi f$):

$$P(t) \propto \tilde{P}(t) = e^{-\omega t/Q}. \quad (6)$$

A similar equation for coda energy was also derived by Dainty (1985).

The logarithmic amplitude plot (Fig. 5) shows that the dependence (6) fits the observed coda amplitudes throughout 100–150 sec of the coda. These linear trends of $\ln P(t)$ are consistent with log-rms coda shapes of Semipalatinsk nuclear explosions presented by Baumgardt (1985). From these trends, we estimate the quality factor as $Q = 320$ near 2 Hz and $Q = 430$ around 5 Hz (Fig. 5).

Although we did not attempt to carry out a rigorous study of frequency-dependent attenuation, the two values above suggest a dependence of $Q \approx 270 \cdot f^{0.3}$. This moderate increase of Q with frequency agrees with values obtained for stable tectonic areas, such as the central US (Nuttli, 1982), the Canadian Shield (Hasegawa, 1985), or central France (Campillo, 1987). The resulting coda Q estimates are consistent with the values characteristic for the crust and support our association of the coda with *Lg* (Singh and Herrmann, 1983; Dainty, 1990). The comparatively low values of $Q \approx 270$ at 1 Hz might be related to the effect of the thick sedimentary cover of the Pechora basin sampled by the part of the profile used in this analysis (Morozova *et al.,* 1999). However, this suggestion needs to be verified by a more detailed analysis.

Decomposition of PNE Energy

The second problem posed in the Introduction, that of apparently much stronger coda of WG_{fs} compared to that of $P_{410}P$ (Fig. 3), is resolved by the observation that the whispering-gallery phases arrive on top of the extensive codas of the preceding arrivals, resulting in buildup of the recorded energy. Thus the observed, overlapping amplitude pattern in Figure 3 must be "deconvolved" in order to extract the actual onset and coda amplitudes of the separate arrivals.

For a simple estimate of the actual arrival amplitudes, we model each of the events as a superposition of a primary arrival and of its coda (Fig. 6). We assume that coda power follows the time dependence (6) and is proportional to the total energy of the primary phase. This approximation leads to a two-parameter amplitude decay model for each of the four arrivals labeled in Figure 3:

$$P(t - t^0) = \begin{cases} 0, & t < t^0, \\ \lambda P^0 \tau \tilde{P}(t - t^0), & t \geq t^0, \end{cases} \quad (7)$$

where t^0 is the onset time, P^0 is the squared amplitude of the onset, τ is the estimated duration of the primary phase (so that $P^0\,\tau$ measures its total energy), and λ is the relative coda amplitude parameter. Since we assume that the mechanism of scattering is common for all arrivals, λ is the same for P, $P_{410}P$, *WG*, and WG_{fs}. Thus the cumulative coda power at time t after the onset of WG_{fs} is:

$$P_{\text{coda}}(t) = P_P(t - t^0_P) + P_{P410P}(t - t^0_{P410P}) + P_{WG}(t - t^0_{WG}) + P_{WG_{fs}}(t - t^0_{FG_{fs}}) + P_{\text{instr}}. \quad (8)$$

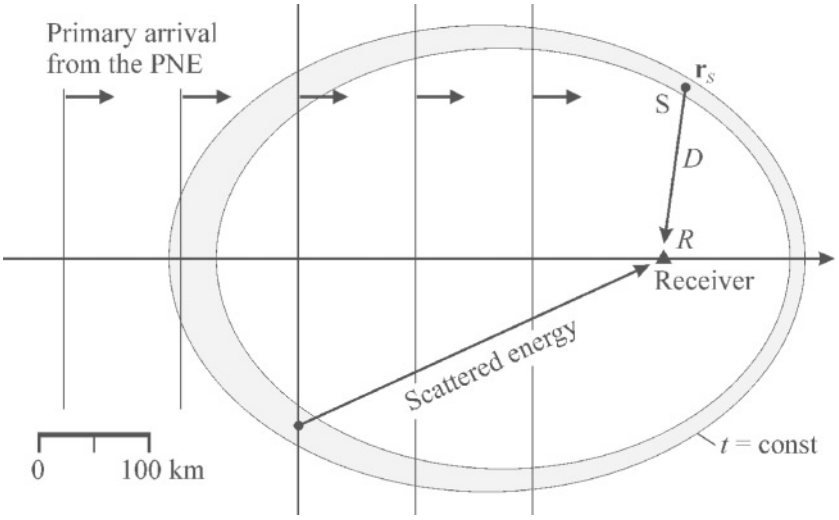

Figure 4. Plan view showing surface area (shaded) of the crust contributing to the coda of the long-range P_n at 50 sec after the onset of this phase at the receiver. The PNE is located at 2500 km from the receiver, and the curvature of the incident wavefronts is ignored for simplicity. In this approximation, the scattering area is bounded by two ellipses t = const. Note that an increasing-with-time source area compensates for the geometric spreading of coda energy. For infinite velocity of the primary phase, the scattering area becomes circular, leading to cancellation of geometric spreading in the simplified equation (6). This plot illustrates the notation in integral (5).

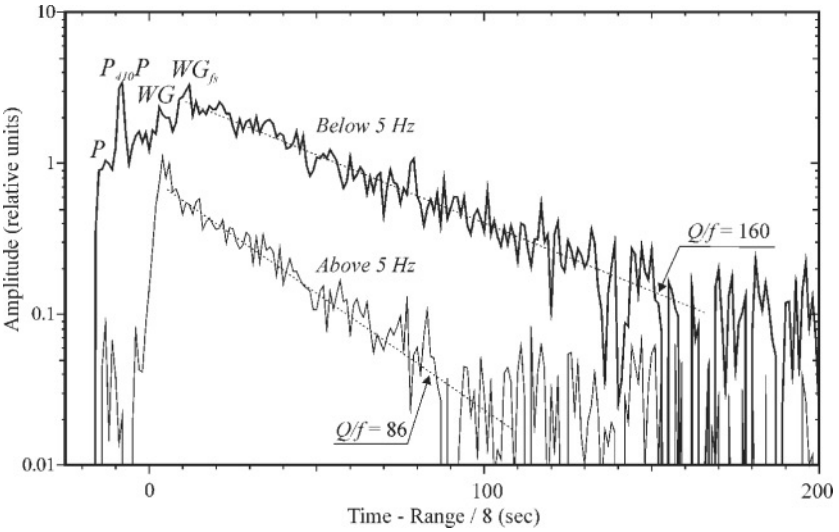

Figure 5. The same amplitudes as in Figure 3 plotted in logarithmic scale. Straight lines correspond to the relation (6) with $Q \approx 320$ for the low-frequency curve (at approximately 2 Hz) and $Q \approx 430$ for high frequency (at 5 Hz). Background noise estimated from a time window between 300 and 350 sec of the records was subtracted from both records prior to taking logarithm.

In expression (8), we include an additive term P_{instr} describing the noise level of the instrument and of the recording site. We estimated this term from measurements of signal amplitude between 300 and 350 sec after the onset of the long-range P_n (the coda practically dissipates after about 150–200 sec; see Figure 3).

Figure 3 shows that the $P_{410}P$ onset is sharper than those of the two *WG* modes. This comparative sharpness is expected because the *WG* modes enter the crust at larger angles, undergo additional reflections from the free surface and from the Moho, propagate within (most likely) a more complex lithospheric structure, and thus should be more subject to perturbations. In our amplitude modeling, we reflect this sharpness by setting the duration of the *P* and $P_{410}P$ onsets equal to half of the duration of the *WG* and WG_{fs} modes. Note that the values τ and λ enter relations (7) only through their product, and thus the accurate absolute values of τ are not critical for coda modeling. We set $\tau = 2.5$ for the two *WG* modes and $\tau = 1.25$ for *P* and $P_{410}P$ phases.

By varying the remaining parameters corresponding to the four amplitudes and λ in relations (7) and (8) in order to match the observed amplitude variations, we obtained in the amplitude units of Figure 3: $A_{\text{P}} \approx 1.7$, $A_{P410P} \approx 4.1$, $A_{WG} \approx 2.1$, $A_{WG_{\text{fs}}} \approx 2.9$, $\lambda \approx 0.22$. During this inversion, we also found that a value of $Q = 380$ better describes the observed pattern of overlapping codas than the value of $Q = 320$ estimated from the cumulative linear trend in Figure 5.

Figure 7 shows that the simple model (7)–(8) describes the observed amplitude pattern satisfactorily throughout the entire recording time range. As expected, the strongest phase in the "deconvolved" amplitude pattern in the bottom of Figure 7 is the reflection from the 410-km discontinuity. Note that because of increased attenuation below about 150-km depth (Morozov *et al.,* 1998a,b), the arrivals from the mantle transition zone are very weak in the high-pass filtered records and they do not boost the apparent *WG* energy (Fig. 3). Therefore, the high-frequency coda of the *WG* arrival in Figure 3 can be directly compared to our modeled *WG* coda

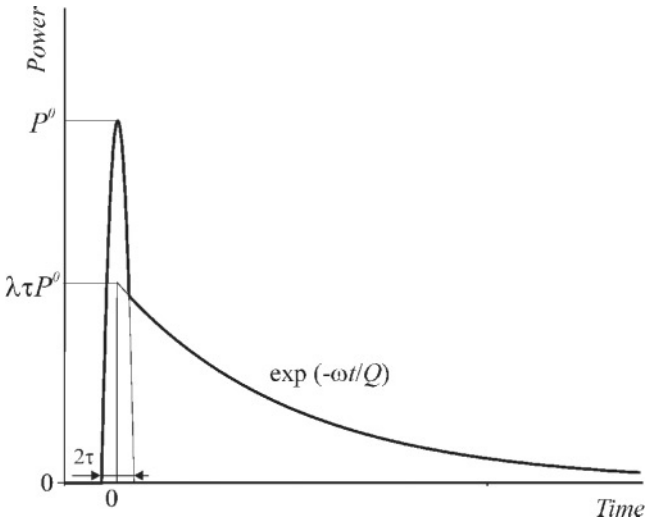

Figure 6. A model of intensity variation with time for a PNE event (see equations (7)). The energy of the primary event is approximated by a parabolic function and is characterized by its peak power P^0 and duration τ. The coda is parameterized by its coupling to the primary event λ and by its decay rate ω/Q defined in relation (6).

in Figure 7. As expected, the low-frequency component of the *WG* phase is still stronger than the high-frequency part, reflecting the source spectrum dominated by the energy between 1 and 2.5 Hz (Morozov *et al.,* 1998b).

Energy Pattern of PNE Wavefield

As the previous argument shows, the energies of secondary phases including the long-range P_n appear stronger than they are in reality due to their enhancement by the codas of the earlier phases. This observation helps us answer the second question posed in the Introduction. However, even after our amplitude correction, the amplitudes of the *WG* modes, and in particular, their total energy (Fig. 7, bottom) are still significantly higher than expected from 1D modeling (Mechie *et al.,* 1993; Morozova *et al.,* 1999). At longer ranges, high amplitudes of the surface multiples of P_n in this region are also indicated by the observations of a very strong *PP* phase (corresponding to the first phase in the WG_{fs} group in our notation) from the Semipalatinsk nuclear explosions (Baumgardt, 1985, 1990).

As a solution to this controversy, we consider two possible factors that could cause the increased energy of the WG modes and that cannot be accounted for in 1D simulations. First, for a PNE near 700-m depth (Sultanov *et al.,* 1999) the *P*-wave energy radiated at about 2-Hz frequency range (the dominant frequency of QUARTZ explosions; cf. Ryberg *et al.,* 1995; Morozov *et al.,* 1998b) is enhanced due to constructive interference with the *pP* reflection from the free surface (Greenfield, 1971). This interference would focus the energy in a downward direction increasing this energy by a factor of 10–13 compared to a source in an infinite medium (note that such interference might account for the 2-Hz peak frequency of the recorded energy). However, a point source is an oversimplified representation for a real explosion, and any irregularity of the source region or nonlinear effects would reduce such focusing (Greenfield, 1971). As a result, 1D modeling tends to overestimate the downgoing energy at the expense of the modes propagating subhorizontally. For an explosion detonated within a heterogeneous crust, we expect that a larger portion of energy would propagate in the form of the lithospheric-guided waves than predicted in 1D simulations.

Another explanation for high amplitudes of the waves guided within the lithosphere could be their focusing under the northern part of the East European Platform. This region has a mantle structure that is distinctly different from that of the West Siberian basin (Mechie *et al.,* 1997; Morozova *et al.,* 1999 and personal communication). The unusually high amplitudes of the long-range P_n have been observed only on the profiles QUARTZ and RUBIN traversing the East European platform (Ryberg *et al.,* 1995), and the strong *PP* phase was also identified practically along the path of the profile RUBIN (Baumgardt, 1985). On the contrary, our preliminary study (the Siberian PNE profiles have not been analyzed in full) suggests that the long-range P_n is much weaker and crustal attenuation is somewhat lower under the Siberian craton (Fig. 8).

Although the previous argument is only qualitative, note that not only the *WG* arrivals but also their primary phases P_n, and P_N (the latter are refractions and reflections from regional seismic boundaries between 90 and 140 km depth; cf. Pavlenkova, 1996; Morozova *et al.,* 1999) are very strong between the offsets of about 300–800 km (Fig. 2). Such strong amplitudes should be due to high energy of the source and to the velocity gradient and reflectivity observed within the lithosphere (Morozova *et al.,* 1999). After a reflection from the Moho and free surface, this near-critical energy could form the observed strong waveguide arrivals (Fig. 3).

Discussion

Since our coda decay model in equation (6) is dictated simply by the scattering geometry and by the principle of conservation of energy, it should be applicable to other observations of scattering at teleseismic distances. Indeed, in a teleseismic study of underground nuclear explosions at Novaya Zemlya, Greenfield (1971) interpreted the observed coda as a result of near-source $Rg \rightarrow P$ scattering and pointed out that without crustal attenuation, the coda energy would have been constant. Dainty (1990) suggested that for Kazakh nuclear tests recorded at NORESS, about half of the coda energy consisted of near-source $Lg \rightarrow P$ scattering, and another half was represented by $P \rightarrow Lg$ scattering near the seismic array, with an energy decay law similar to derived above (Dainty, 1985). Baumgardt (1985, 1990) used incoherent beams and continuous "polar scans" to identify var-

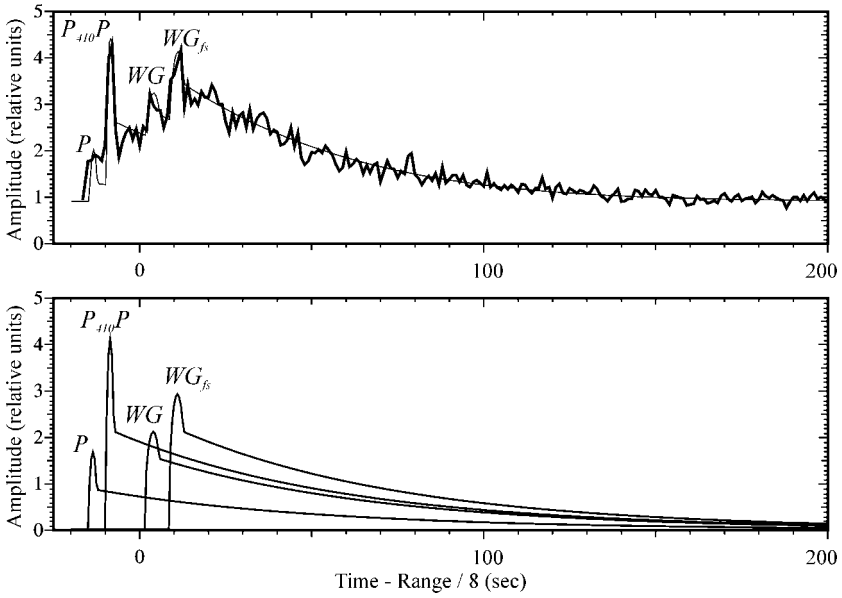

Figure 7. (Top) Coda amplitude decay model for frequencies below 5 Hz (Fig. 3). Thick line is the low-frequency amplitude from Figure 3, thin line shows the modeled amplitude decay described by relation (8). Note that crustal scattering and a simple approximation of coda power (1) explain the observed coda build-up by the subsequent P, $P_{410}P$, WG, and WG_{fs} arrivals. (Bottom) Amplitudes and codas of the four separate arrivals forming the total coda energy (8). Note that this decomposed section is dominated by the reflection $P_{410}P$. Also compare the amplitude of WG in this plot to the high-frequency WG coda in Figure 3 and note that WG is stronger at lower frequencies, as expected.

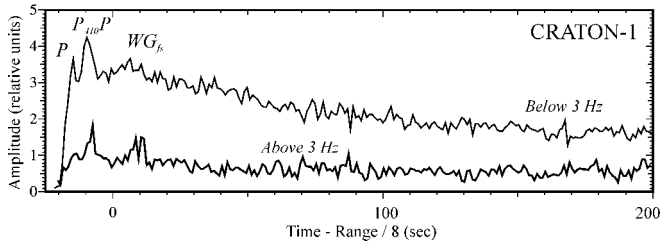

Figure 8. Records from PNE CRATON-1 in the West Siberian basin averaged and plotted in the same way as QUARTZ-4 records in Figure 3. Due to lower frequency content of these records, the frequency band separation is performed at 3 Hz instead of 5 Hz in Figure 3. Note that even without correcting for coda build-up, the WG_{fs} is weaker than $P_{410}P$ and also much weaker than in the records from QUARTZ-4 (Fig. 3). Also note the longer codas and increased high-frequency content of WG_{fs} (compared to WG), in contrast to Figure 3. These differences suggest regional variations in WG propagation characteristics and lower crustal attenuation within the Siberian craton.

iations in coda decay and mode content within 200–400 sec of the teleseismic P-wave codas.

Although the density of PNE recordings (10–15 km spacing) does not allow application of array methods for a detailed identification of the constituents of the coda (e.g., Bannister *et al.,* 1990; Hedlin *et al.,* 1994), the length of recording and the extent of coverage (Fig. 2) allow measurements of the coda decay rate. Our model (Fig. 7) shows that crustal-guided waves explain not only its amplitude decay but also the apparent lack of a pronounced coda of the body-wave arrivals from the mantle transition zone. Due to the slow coda amplitude decay rate, the codas of the PNE arrivals can be observed to 100–150 sec, and therefore the codas of multiple P-wave arrivals overlap and boost the energy of the later arrivals including the long-range P_n.

The coda of the WG phases and, as we suggested previously, of all the other P-wave phases are not due to anomalously low crustal attenuation and to a tuned, narrowband, highly scattering uppermost mantle as suggested by Ryberg *et al.* (1995) or by Ryberg *et al.* (1999). The coda is neither unusually high-frequency nor long to require such an interpretation. On the contrary, we favor the traditional interpretation of the coda as a result of crustal scattering of the waves incident from the mantle and propagating at high apparent velocities. The reciprocity principle complements this mechanism by its counterpart in which strong crustal-guided waves (*Pg, Sg, Lg, Rg*) generated by the PNE are scattered on crustal heterogeneities producing secondary phases propagating through the mantle and feeding the observed coda (Dainty, 1985, 1990).

Although our "instantaneous distributed coda source" model (6) is only an approximation to the actual spreading coda source region, it is clearly more adequate than the point-source scheme (1) used by Ryberg *et al.,* (1995) and Ryberg and Wenzel (1999). The relative velocities of the fast primary (P_n) to the slow scattered (*Lg, Rg*) phases lead to a distributed scattering mechanism and to the cancellation of the geometric factor in our coda decay relation (6). On the contrary, although the model by Ryberg *et al.* (1995) and Ryberg and Wenzel (1999) also implied distributed scattering (in their case, located within the mantle), these authors made no attempt to derive a proper coda relation for this scattering geometry. Instead, they resorted to a model of coincident coda source and receiver (Aki and Chouet, 1975) that is totally irrelevant in this case.

While attributing all scattering to the crust and Moho boundary, our argument does not eliminate the possibility of mantle scattering. Some degree of scattering should certainly

be present in the uppermost mantle, yet such scattering is not required by the observations of PNE coda. At the same time, mantle scattering cannot be as high as suggested in the model by Ryberg and Wenzel (1999) in which the 75-km thick sub-Moho mantle reflects about 8–10 times more seismic energy than the Moho (as estimated by Morozov, in press). Such strong scattering would most certainly destroy any coherent seismic waves penetrating through the uppermost mantle.

Our estimates of arrival amplitudes suggest that the dominance of the *WG* modes in the energy pattern of the PNE wavefield is to a certain degree apparent. Despite the high values of the observed amplitudes within the long-range P_n time window (Fig. 3), both of the *WG* modes actually carry only about 75% of the power delivered to the surface by the $P_{410}P$ reflection. Since the $P_{410}P$ reflection is more coherent and shorter in duration, its coda is somewhat lower in amplitude, yet it carries about 65% of the energy of both *WG* codas and about the same as the WG_{fs} coda alone.

Being significantly lower than it appears, the energy of the *WG* modes is still high compared to the predictions of 1D simulations. As we suggested previously, 1D modeling of a PNE as a point source in a homogeneous crust could underestimate the amount of energy propagating in seismic phases guided within the crust and lithosphere. However, considering the uniqueness of the observation of high-energy long-range P_n under the East European platform and the West Siberian Basin, our preferred explanation of such high amplitudes is their being caused by focusing in these regions.

The high amplitudes of multiple refractions (*PP* and *WG*) could be qualitatively explained by the effects of crustal, Moho, and lithospheric heterogeneity favoring propagation of energy within the top 150–200 km of the mantle under the northern part of the East European platform and under the West Siberian basin (Fig. 1). Among these effects are the strong velocity gradient and reflecting boundaries in the uppermost mantle (Morozova *et al.,* 1999). As demonstrated by Kennett (1987), within the ranges of PNE profiles (20° to 30°), layered structures within the mantle may act as a wave guide contributing significantly to the *P*-wave coda.

Baumgardt (1985) also suggested that focusing could explain the high-amplitude *PP* in NORSAR recordings of the Semipalatinsk nuclear explosions. In particular, near-receiver focusing was required to account for the variations of *PP* amplitude across the array. In contrast to this observation, QUARTZ records show consistent and strong *WG* phases within the entire offset range and suggest that reflective lithosphere with vertical velocity gradient and favorable source conditions should be responsible for the overall character of the wavefield. Near-receiver scattering manifests itself in reduced coherency between the adjacent seismograms.

The unusually strong P_n and *WG* phases observed in QUARTZ records could support the observations of coda flattening between 310 and 450 sec after the teleseismic *P*-wave arrival in the recordings of Semipalatinsk explosions at NORSAR (Baumgardt, 1985, 1990). In a detailed study, Baumgardt (1990) showed that this part of the coda consisted primarily of *Lg* and S_n modes, with minor amounts of P_n energy and no detectable teleseismic *P* contribution. He interpreted this coda flattening as a result of $P_n \rightarrow Lg$ scattering under the Urals. This explanation, which appears to be the only reasonable model of the observed coda, also implies that the P_n is strong and carries enough energy to reverse the decay of the *P*-wave coda.

The observed difference between the amplitude dependencies of the records at lower and higher frequencies (Fig. 5) is very significant. Similarly to the deep *P*-wave phases, the WG_{fs} arrival and its coda are low in their high-frequency content (Fig. 5). Compared to *WG,* WG_{fs} is similar but travels two additional passes through the crust, and thus the disappearance of WG_{fs} in the high-pass filtered record should be related to crustal attenuation. Also, the increased *Q* at higher frequencies (Fig. 5) and its regional variations (Fig. 8) suggests that the low-frequency coda contains more surface waves sampling the sedimentary, lower-*Q* parts of the upper crust. Therefore, the difference between *WG* and WG_{fs} also points to a crustal nature of the coda.

An important implication of our coda model is that only a three-dimensional (3D) analysis of scattering can yield reasonable quantitative estimates of the dynamic properties of the PNE wavefield. Although 3D or 2D modeling of PNE short-period records using realistic crustal and mantle models is at present not practical, it appears that interpretations of scattering based exclusively on 1D simulations (Tittgemeyer, 1996; Ryberg and Wenzel, 1999) might be misleading. On the contrary, energy balance considerations consistent with the accepted teleseismic coda models and utilizing the true, 3D view of the process of wave propagation allow us to explain the behavior of the coda and to unravel the amplitude relations between the observed PNE phases.

Conclusions

The work presented above focused on the observed properties of the long-range PNE phases, and particularly, on the strong amplitude and long duration of the coda of the long-range P_n. Reconsidering the available observations of this phase in the records from the PNE profile QUARTZ, we arrived at both a consistent explanation of the character of this coda as well as at a realistic estimate of its decay rate, in contrast to some of the previous results (Ryberg *et al.,* 1995; Tittgemeyer *et al.,* 1996; Ryberg and Wenzel, 1999). The key points of our coda model of PNE arrivals are:

1. Regardless of the accepted explanation for the nature of the long-range P_n, a long coda is not specific to this phase but it follows every PNE arrival at an offset range over 2000 km.
2. The 100- to 150-sec-long codas of the long-range arrivals are due to the generation of these codas within the crust

by PNE phases propagating at high apparent velocities thus leading to distributed coda excitation and reduced geometric spreading.

3. The codas of the PNE arrivals build up energy within the record section leading to an increased energy within the long-range P_n time window; the amplitude pattern of the records was inverted for true amplitude relations between the arrivals.

Based on a detailed analysis of the long-range P_n, we demonstrated that this phase consists of two groups of arrivals that are clearly distinct in their frequency, amplitude, coda, and travel-time patterns. On the weight of such combined evidence, these arrivals are explained as the Moho and free-surface multiples of the refractions and reflections within the uppermost-mantle (P_n, P_N).

As a result of our PNE coda model, we obtained estimates of coda Q ranging between $Q = 380$ near 2 Hz and $Q = 430$ around 5 Hz. These values correspond to the values generally associated with the crust (including the sedimentary rocks) and suggest that the crust could be the source of the extensive coda pattern observed in PNE records (Fig. 2). As our study shows, the amplitude pattern of the PNE records throughout their full length can be explained quantitatively by body- and guided waves within the upper mantle and by (predominantly) crustal scattering.

Acknowledgments

This work was performed at the University of Wyoming reflection seismology laboratory. We thank Drs. Harley Benz, Gene Humphreys, Elena Morozova, and Mark Tittgemeyer for numerous discussions of the properties of the long-range P_n. Reviews by Dr. Douglas Baumgardt and by the Associate Editor Dr. Anton Dainty helped to improve the argument, bibliography, and presentation of this article. Our research was sponsored by the Air Force Office for Scientific Research Grants F49620-94-1-0134 and F49620-94-A-0134 and by the Defense Threat Reduction Agency Grant DSWA01-98-0015.

References

Aki, K., and B. Chouet (1975). Origin of coda waves: source, attenuation, and scattering effects, *J. Geophys. Res.* **80,** 3322–3342.

Bannister, S. G., E. S. Husebye, and B. O. Ruud (1990). Teleseismic *P* coda analyzed by three-component and array techniques: deterministic location of topographic *P*-to-*Rg* scattering near the NORESS array, *Bull. Seism. Soc. Am.* **80,** 1969–1986.

Baumgardt, D. R. (1985). Comparative analysis of teleseismic *P* coda and *Lg* waves from underground nuclear explosions in Russia, *Bull. Seism. Soc. Am.* **75,** 1413–1433.

Baumgardt, D. R. (1990). Investigation of teleseismic *Lg* blockage and scattering using regional arrays, *Bull. Seism. Soc. Am.* **80,** 2261–2281.

Bostock, M. G. (1998). Mantle stratigraphy and evolution of the Slave province, *J. Geophys. Res.* **103,** 21,183–21,200.

Campillo, M. (1987). *Lg* wave propagation in a laterally varying crust and the distribution of the apparent quality factor in central France, *J. Geophys. Res.* **92,** 12604–12614.

Campillo, M. (1990). Propagation and attenuation characteristics of the crustal phase *Lg, Pageoph.* **132,** 1–17.

Dainty, A. M. (1985). Air Force Geophysical Laboratory Report, AFGL-TF-86-0218.

Dainty, A. M. (1990). Studies of coda using array and three-component processing, *Pageoph* **132,** 221–244.

Der, Z. A., A. C. Lees, and V. F. Cormier (1986). Frequency dependence of *Q* in the mantle underlying the shield region of Eurasia. III. The *Q*-model, *Geophys. J. R. Astr. Soc.* **87,** 1103–1112.

Enderle, U., M. Titgemeyer, M. Itzin, C. Prodehl, and K. Fuchs (1997). Scales of structure in the lithosphere: images of processes, *Tectonophysics* **275,** 165–198.

Frankel, A., A. McGarr, J. Bicknell, J. Mori, L. Seeber, and E. Cranswick (1990). Attenuation of high-frequency shear waves in the crust: measurements from New York state, South Africa, and southern California, *J. Geophys. Res.* **95,** 17,441–17,457.

Fuchs, K., and G. Müller (1971). Computation of synthetic seismograms with the reflectivity method and comparison with observations, *J. R. Astr. Soc.* **23,** 417–433.

Greenfield, R. J. (1971). Short-period *P*-wave generation by Reileigh-wave scattering at Novaya Zemlya, *J. Geophys. Res.* **76,** 7988–8002.

Gupta, I. N., T. W. McElfresh, and R. A. Wagner (1991). Near-source scattering of Raylegh to *P* in teleseismic arrivals from Pahute Mesa (NTS) shots, in *Explosion Source Phenomenology,* S. R. Taylor, H. J. Patton, and P. G. Richards (Editors), *American Geophysical Monograph* **65,** 151–160.

Hasegawa, H. S. (1985). Attenuation of *Lg* waves in the Canadian Shield, *Bull. Seism. Soc. Am.* **75,** 1569–1582.

Hedlin, M. A. H., J.-B. Minster, and J. A. Orcutt (1994). Resolution of prominent crustal scatterers near the NORESS small aperture array, *Geophys. J. Int.* **119,** 101–115.

Henstock, T. J., A. Levander, C. M. Snelson, K. G. Miller, S. H. Harder, A. R. Gorman, R. M. Clowes, M. J. A. Burianyk, E. G. Humphreys (1998). Probing the Archean and Proterozoic lithosphere of western North America, *GSA Today* **8,** 1–5.

Kennett, B. L. N. (1987). Observational and theoretical constraints on crustal and upper mantle heterogeneity, *Phys. Earth Planet. Interiors* **47,** 319–332.

McNamara, D. E., T. J. Owens, and W. R. Walter (1996). Propagation characteristics of *Lg* across the Tibetian Plateau, *Bull. Seism. Soc. Am.* **86,** 457–469.

Mechie, J., A. V. Egorkin, K. Fuchs, T. Ryberg, L. Solodilov, and F. Wenzel (1993). *P*-wave velocity structure beneath northern Eurasia from long-range recordings along the profile Quartz, *Phys. Earth Planet Interiors* **79,** 269–286.

Mechie, J., A. V. Egorkin, L. Solodilov, K. Fuchs, F. Lorenz, and F. Wenzel (1997). Major features of the mantle velocity structure beneath northern Eurasia from long-range seismic recordings of peaceful nuclear explosions, in Upper mantle heterogeneities from active and passive seismology, K. Fuchs (Editor), Kluwer Academic Publ., Dordrecht, pp. 33–50.

Morozov, I. B. Comment on "High-frequency wave propagation in the uppermost mantle" by T. Ryberg and F. Wenzel, *J. Geophys. Res.,* in press.

Morozov, I. B., and S. B. Smithson (1996). Instantaneous polarization attributes and directional filtering, *Geophysics* **61,** 872–881.

Morozov, I. B., E. A. Morozova, and S. B. Smithson (1998a). On the nature of the teleseismic *Pn* phase observed in the recordings from the ultra-long profile "Quartz", Russia, *Bull. Seism. Soc. Am.* **88,** 62–73.

Morozov, I. B., E. A. Morozova, S. B. Smithson, and L. N. Solodilov (1998b). 2-D image of seismic attenuation beneath the Deep Seismic Sounding profile "Quartz", Russia, *Pure Appl. Geophys.* **153,** 311–348.

Morozova, E. A., I. B. Morozov, S. B. Smithson., and L. N. Solodilov (1999). Heterogeneity of the uppermost mantle beneath Russian Eurasia from the ultra-long range profile QUARTZ, *J. Geophys. Res.* **104,** no. B9, 20,329–20,348.

Nuttli, O. W. (1982). The earthquake problem in the eastern United States, *J. Struct. Div. Am. Soc. Civ. Eng.* **108,** 1302–1312.

Pavlenkova, N. I. (1996). General features of the uppermost mantle strati-

fication from long-range seismic profiles, *Tectonophysics* **264,** 261–278.

Ryberg, T., and F. Wenzel (1999). High-frequency wave propagation in the uppermost mantle, *J. Geophys. Res.* **104,** 10,655–10,666.

Ryberg, T., K. Fuchs, A. V. Egorkin, and L. Solodilov (1995). Observations of high-frequency teleseismic P_n on the long-range Quartz profile across northern Eurasia, *J. Geophys. Res.* **100,** 18,151–18,163.

Ryberg T., M. Tittgemeyer, and F. Wenzel (1999). Propagation of elastic waves in the uppermost mantle, AGU Fall Meeting, San Francisco, California F712, *EOS Trans. Am. Geophys. Union* (Suppl.) **80,** no. 46.

Singh, S., and R. B. Herrmann (1983). Regionalization of crustal coda Q in the Continental United States, *J. Geophys. Res.* **88,** 527–538.

Sultanov, D. D., J. R. Murphy, and Kh. D. Rubinstein (1999). A seismic source summary for Soviet Peaceful Nuclear Explosions, *Bull. Seism. Soc. Am.* **89,** 640–647.

Thybo, H., and E. Perchuc (1997). The seismic 8° Discontinuity and Partial Melting in Continental Mantle, *Science* **275,** 1626–1629.

Tittgemeyer, M., F. Wenzel, K. Fuchs, and T. Ryberg (1996). Wave propagation in a multiple-scattering upper mantle: observations and modeling, *Geophys. J. Int.* **127,** 492–502.

Department of Geology and Geophysics
Rice University
MS-126, 6100 South Main Street
Houston, Texas, 77005-1892
morozov@geophysics.rice.edu
(I. B. M.)

Department of Geology and Geophysics
University of Wyoming
PO Box 3006
Laramie, Wyoming 82071-3006
(I. B. M., S. B. S.)

Manuscript received 3 September 1999.